Anistropic electron-electron and electron-phonon scattering rates in aluminium from high-precision RFSE measurements between 0.2 and 10 K

1994 J. Phys.: Condens. Matter 6 11081

(http://iopscience.iop.org/0953-8984/6/50/017)

J. Phys.: Condens. Matter 6 (1994) 11081–11098. Printed in the UK

Anisotropic electron–electron and electron–phonon scattering rates in aluminium from high-precision RFSE measurements between 0.2 and 10 K

A Jaquier, P A Probst and R Huguenin
Institut de Physique Expérimentale, Université de Lausanne, CH-1015 Lausanne, Switzerland

Received 15 July 1994, in final form 3 October 1994

Abstract. High-precision low-temperature radio frequency size effect (RFSE) experiments have been carried out to extract local values of the electron–phonon (e–p) and electron–electron (e–e) scattering rates (SRs) in aluminium. The RF was varied to help separate these two contributions. For the first time an unexpected large anisotropy of the e–e SR has been observed, suggesting that the phonon mediated e–e SR dominates the Coulomb contribution. Comparison of the experimental data with recent calculated values of the e–e SR confirm the importance of this mechanism.

1. Introduction

Considerable efforts have been devoted to the problem of the interaction between the electrons in metals but our understanding of the subject is far from complete and new information from experiment and theory is still needed.

The search for experimental evidence of electron–electron (e–e) scattering started soon after Landau and Pomeranchuk, and somewhat later Baber, showed that it should be the ultimate temperature dependent mechanism contributing to the dissipation of the electrical current at low temperature (Baber 1937, Landau and Pomeranchuk 1936). It appears as a T^2 component that was observed soon after its prediction in the electrical resistivity of many transition metals and alloys, but only recently in 'simple' metals, such as K, Cu and Al. The magnitude of the T^2 term in the electrical resistivity, in units $\Omega m\ K^{-2}$, ranges from a huge 3.5×10^{-7} in the heavy-fermion compound $CeAl_2$ to 10^{-10} or 10^{-11} in A15 compounds, 10^{-13} in transition metals, down to about 10^{-15} in 'simple' metals. The latter value is obviously difficult to determine and this was only possible when modern high-resolution measuring techniques became available (Ribot *et al* 1981). While the origin of the T^2 terms in heavy-fermion systems and A15 compounds is still controversial, Potter and Morgan have given a convincing explanation for the high e–e resistivity ρ_{ee} in transition metals (Potter and Morgan 1979). They showed in particular that the Coulomb interaction properly describes the anisotropy observed in W and Schwartzman and Lawrence found that the phonon mediated e–e interaction produces an excellent agreement between theory and experiment in six transition metals (Mo, W, Nb, Ru, Os and Re) and two simple metals (Cd and Al) (Schwartzman and Lawrence 1993).

Quite a number of problems are associated with the comparison of ρ_{ee} from theory and experiment. ρ_{ee} results from averages over the whole Fermi surface (FS) and is difficult to calculate, in particular because momentum conservation makes normal e–e collisions ineffective and the electrical resistivity of uncompensated metals is only affected if a

0953-8984/94/5011081+18$19.50

reciprocal vector G is involved in the process. It follows that one has to determine the relative importance of umklapp to total scattering and this is in general not very well known. From the experimental point of view the coefficient of the T^2 term to be compared with theory has to be disentangled from the usually much larger e–p contribution, with possible interference between different scattering mechanisms, known as deviations from Matthiessen's rule. It is moreover very often sample dependent due to enhancement from dislocations (see the review by Kaveh and Wiser (1984)).

A better detailed comparison with theory is expected from experimental techniques also able to look at the anisotropy of e–p or e–e scattering and at its temperature dependence (Gasparov and Huguenin 1993). Several selective methods indeed give access to local SRs or orbital averaged SRs. As they all require high-quality crystals with a SR smaller than 10^{-10} s^{-1} (a mean free path of a few tenth of a millimetre), their use is limited to pure metals at low temperatures. Among these techniques, surface Landau level (SLL) and Azbel–Kaner cyclotron resonance (AKCR) experiments allow the determination of the SR from the line shape of a resonance signal at well defined values of a magnetic field, while in the RFSE it is the amplitude of the resonance that is related to the SR. The electric radio frequency (RF) field used in all these methods is non-zero in the skin depth only, so most of the carriers are in thermal equilibrium, which gives these methods their selectivity for local SRs and makes them free from deviations from Matthiessen's rule (Wagner and Bowers 1978).

In the seventies the accuracy on the amplitude of the RFSE signal was limited to a few per cent, so that in simple metals only e–p scattering could be studied (see the reviews by Gantmakher and by Wagner and Bowers (Gantmakher 1974, Wagner and Bowers 1978)). In good experimental conditions the e–p SR consistently followed a simple T^3 law, as predicted from the Debye model, although deviations from the cubic dependence are expected in metals with multiple FS sheets. Moreover the anisotropy of the e–p SR was found to be a general rule, which follows from the shapes and curvatures of the FS together with the anisotropy of the phonon spectrum. The accuracy at the level of a few per cent was enough though to study e–e scattering in transition metals (Boiko *et al* 1974). In the late eighties, however, RSFE experiments were improved considerably and their high stability has allowed the investigation of e–e scattering in noble metals (Stubi *et al* 1988a) and in Cd (Jaquier *et al* 1991) (see also the review by Gasparov and Huguenin (1993)).

Al is a good candidate for comparison between theory and experiment. It is a simple metal with s and p conduction electrons on two FS sheets, well described by a simple 4-OPW model (Ashcroft 1963), and a theoretical phonon spectrum resulting from a fit to neutron data (Hartmann and Milbrodt 1971). On the other hand the metallurgy of Al is well under control and high-purity samples can be prepared.

However the electrical resistivity data of Al at low temperature were for a long time quite confusing until high-resolution (10^{-7}) measurements were reported (Ribot *et al* 1981) demonstrating that below 3 K $\rho(T)$ can be analysed in terms of a superposition of two contributions, $\rho(T) = AT^2 + BT^5$, with $A = 2.8 \times 10^{-15}$ Ω m K^{-2} and $B = 5 \times 10^{-17}$ Ω m K^{-5}. Recently this interpretation was questioned (Hou and Kos 1993) and a reanalysis of Ribot *et al*'s data produced a 50% larger A. In any case the value of A is about 20 times larger than the value predicted by Lawrence and Wilkins (1973) in their calculation of the e–e resistivity. This order of magnitude difference was explained later on by MacDonald, who showed that the e–p coupling is sufficiently strong in superconducting metals for the e–e SR to be dominated by phonon mediated transitions (MacDonald 1980). From this mechanism he calculated for Al a new value of $A = 4.1 \times 10^{-15}$ Ω m K^{-2}, that is, 20 times larger than Lawrence's value and in close agreement with the experiment. On the other hand the value of B measured by Ribot *et al* is only a factor of three smaller

than calculated (Lawrence and Wilkins 1972) from e–p scattering. In a later microscopic calculation of the e–p SR at a few points of the FS Meador and Lawrence also predicted large anisotropy and showed that the T^3 law expected from the Debye model is not a good description except on the free-electron-like parts of the FS (Meador and Lawrence 1977).

In their SLL measurements in Al Wegehaupt and Doezema observed the predicted anisotropy but found however no deviations from the T^3 law (Wegehaupt and Doezema 1978). Furthermore, they found no sign of the expected e–e term. Using RFSE Parsons and Steele observed at $\nu(T) \propto T^n$ with $n \approx 2.2$–3, but their experimental accuracy was not sufficient to separate the different contributions to the SR (Parsons and Steele 1979). This is also the reason why Gasparov and Harutunian failed in their attempt to detect an e–e SR in Al and in Cu using the same technique (Gasparov and Harutunian 1976).

The precision achieved now ($\approx 10^{-4}$ instead of 10^{-2} previously) in RFSE experiments is high enough to allow a much better separation of the different contributions to the SR, and one can hope to observe effects due to e–e scattering and thus to reconcile the electrical resistivity data with the RFSE data. This gave us the incentive to look at the SR of a few selected groups of charge carriers in Al and to check for the anisotropy of the e–e SR, which would possible occur if phonon mediated transitions are dominant, as suggested by the electrical resistivity results. Simultaneously we also performed a microscopic calculation of the point SRs over the entire FS, described briefly below, in order to be able to compute the orbital averages measured in the RFSE (Jaquier 1994). This will provide a more stringent test of the theory than has been possible until now. At the same time we have completed a detailed map of the effective mass renormalization parameter $\lambda(k)$, and used it to calculate the cyclotron effective masses for extremal orbits for any field direction and the times of flight of the electrons on these orbits.

In the next section we discuss briefly our approach to the calculation of the SRs on well defined orbits on the FS. We then explain anomalies in the temperature dependence of some RFSE amplitudes, also observed in a previous work (Parsons and Steele 1979). In section 3 we describe the experimental set-up, including the multiple-channel digital lock-in amplifier we had to develop and an optimized temperature controller, and in section 4 we present our experimental results on orbits on the second and third zones. The data are discussed in section 5 and compared with theoretical calculations.

2. Scattering rates

2.1. The computation of scattering rates

The details of our computation of the temperature dependent electronic SRs at low temperature, including e–p, e–e phonon mediated and e–e Coulomb scattering, will be published elsewhere and we shall only sketch here a few essential points. The first (i) of these mechanisms is due to the absorption and the emission of real phonons (figure 1(*a*)) the second (ii) to the exchange of virtual phonons (figure 1(*a*)) and the Coulomb interaction (iii) can be represented by the exchange of virtual phonons (figure 1(*c*)). Our virtual phonon calculation is an application to a real metal of the formalism of Schwartzman and Lawrence who treat these processes self-consistently to the second-order expansion of the e–p interaction (Schwartzman and Lawrence 1993).

The first step in the calculation is the description of the FS, by using a 4-OPW model (Ashcroft 1963) fitted (Monnier and Joss 1980) to experimental data. A dense mesh is then built (Meador and Lawrence 1977) for one of the 48 basic elements of symmetry of the cubic centred Brillouin zone. The electron velocities and the density of states are obtained from the same secular equation as the FS, with small corrections for the energy dependence

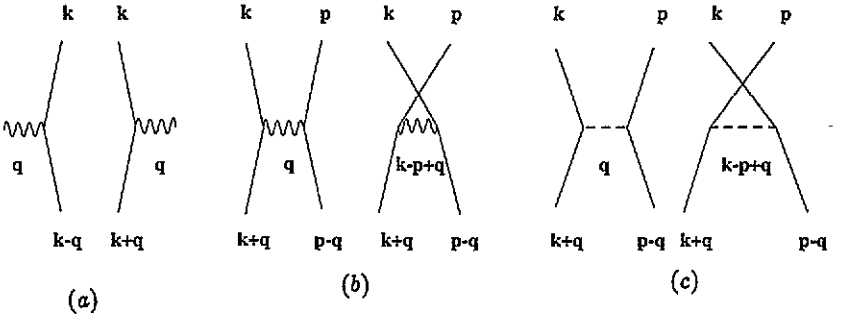

Figure 1. The processes contributing to the electron SR: (*a*) absorption and emission of a real phonon; (*b*) exchange of a virtual phonon (phonon mediated e–e interaction); (*c*) exchange of a virtual photon (Coulomb e–e interaction).

of the pseudopotential. The phonon spectrum is given by a 21-shell model fitted to neutron data, and the e–p interaction is calculated as described by Meador and Lawrence. We have extended their calculation of (i) to cover the entire FS and we have calculated (ii) microscopically for the first time. Contribution (ii) is estimated for the sake of comparison using the Thomas–Fermi model for the underlying interaction while incorporating band structure in the matrix element. Both (ii) and (iii) are quadratic in temperature with (ii) at least an order of magnitude greater, as expected (MacDonald 1980). Furthermore, (ii) is found to be highly anisotropic and (iii) much less so, also as expected. The e–p SR is proportional to T^3 on the nearly free electron regions in the second zone below 15–20 K, but in other regions of the FS the local density of accessible states is responsible for a large variety of T dependences.

We have modelled the trajectories of various groups of electrons from ingredients used in the computation (topology of the FS) or calculated (local electron velocities $v(k)$, normalization factor $\lambda(k)$). This provides a powerful tool to identify RFSE signals arising at particular values and direction of the applied magnetic field. It also allows the determination of the time necessary for the charge carriers to go from one side of the sample to the other and the calculation of orbitally averages SRs from point SRs.

2.2. Scattering rates and experimental conditions

It is now well known that one should choose the experimental conditions carefully in order to determine the SRs from the amplitude $A(T)$ of the RFSE resonance signals (Stubi *et al* 1988a, b, Wagner and Bowers 1978). In particular the following two effects have an influence on $A(T)$, which is usually not negligible.

(i) At low temperatures the e–p SR tends ultimately to the Debye limit that is, the final state k' is in the tangent plane at k, leading to its proportionality to T^3. Our calculation shows that deviations from T^3 may start at low T making the separation of a usually small e-e T^2 term from a complicated T dependent e–p SR difficult. While e–e scattering events involve virtual phonons and retain large-angle character at low temperatures, the e–p events require real phonons, so that the typical scattering angles proportional to $q/k_F \propto T$ become very small at low temperature. However, one can exploit the difference in scattering angles in order to separate the e–e and e–p contributions: by increasing δ/d and using smaller RF and/or sample thickness, one makes small-angle e–p collisions less effective, or almost totally ineffective below about 2 K (Stubi *et al* 1988b), which eases considerably the extraction of the e–e SR.

Table 1. Characteristics of the samples.

Sample	d (μm)	$n \parallel$	ν_0 (s^{-1})	l (μm)	RRR
Al 610	610	(100)	6.9×10^9	450	30250
Al 438	438	(100)	5.8×10^9	510	34300

(ii) The e–p scattering is energy dependent, with a minimum value at the Fermi level. In the jellium model for instance one finds an energy averaged SR

$$\langle \nu \rangle_\varepsilon = \int_0^\infty d\varepsilon \left(-\frac{\partial f_0}{\partial \varepsilon} \right) \nu(\varepsilon, T) = \tfrac{12}{7} \nu(\varepsilon_F). \tag{1}$$

As discussed in the review by Wagner and Bowers (1978), its effect on the RSFE signal amplitude is included in the following expression:

$$\langle A(T) \rangle = A(0) \int d\varepsilon \left(-\frac{\partial f_0}{\partial \varepsilon} \right) \exp\left(-\nu_{ep}(\varepsilon, T) t \right) \tag{2}$$

where t is the sample crossing time. At low T, when $\nu_{ep} t \ll 1$, the energy averaged value is $\frac{12}{7}$ times larger than the value at the Fermi level. At higher T, when $\nu_{ep} t \gg 1$, only electrons with the lowest SR can cross the sample and the SR at the Fermi level is measured. We shall obtain a smooth crossover between these two extreme cases (see section 4) by means of the same model as has been used successfully by Stubi *et al* to explain their data in noble metals (Stubi *et al* 1988b).

3. Experimental details

The measurements were carried out at the two RFs of 2.6 and 0.8 MHz in the temperature range 0.2–10 K in a dilution refrigerator. The sample is clamped between a Cu rod bolted to the He^3–He^4 pot and a small Cu block containing a calibrated Ge resistance thermometer. The horizontal DC magnetic field B produced by an electromagnet is approximately parallel to the sample and its direction is precisely adjusted through a small vertical field of a superconducting solenoid to investigate either central orbits at a given resonance field B_c or quasicentral orbits, which may pass through the skin depth after $n + \frac{1}{2}$ ($n = 1, 2, \ldots$) revolutions inside the sample. We shall see below that this is essential in Al to avoid overlapping of signals from different orbits and moreover it allows the estimate of the mean free path from physical defects and chemical impurities.

3.1. Sample preparation

The difficulty consists in making a sample of about 1 cm^2 with two parallel faces ~500 μm apart, out of a very pure single crystal. The ratio δ/d (skin depth/thickness) accounts for the sensitivity to small-angle scattering and any fluctuation in d has the same effect as a larger δ, i.e. it broadens the resonance signal. In order to obtain narrow resonance lines the thickness has to be constant within ± 1 μm. The starting material is an ingot 13.5 mm in diameter from Vereinigte Aluminium Werke, Germany. As an Al slice about 1 mm thick bows during spark cutting, the crystal is glued on a L shaped support. A hole in the support allows orientation of the sample with x-rays within $\pm 0.5°$, and a thin slice is spark cut. The surface is mechanically polished by moving the crystal gently over an abrasive material† on a flat surface. The polished face is then glued, the other one spark cut and the sample is fixed to a polishing holder, to obtain a good parallelism by mechanical polishing of the second face. Chemical etching with orthophosphoric acid is finally used to remove surface damage. Table 1 lists characteristics of the samples used in this investigation.

† Struers 1000 and 2400A silicon carbide polishing paper, then DP Dur with 1 μm diameter Al_2O_3 paste.

In table 1 n is the sample normal and ν_0 the SR from impurities and physical defects. It has been determined from the ratios of the amplitudes of quasicentral orbits, obtained at slightly different resonance fields, with corresponding real space trajectories consisting of $\frac{1}{2}$, $\frac{3}{2}$, $\frac{5}{2}$, ... turns before the electron reaches the other side of the sample. The amplitudes A_n at resonance fields B_n are related to the mean free path l by the expression $A_n \propto \exp -\{(n+\frac{1}{2})\hbar \int dk/(eB_n l)\}$. $\int dk$ on a complete orbit is the same for all B_n as long as the angle between the field and the sample surface is constant (see Peercy *et al* 1968). The residual resistivity ratios (RRRs) and ν_0 have been calculated from the measured l under the assumption of free electrons.

3.2. Data acquisition

In the absence of multiple revolutions of the electrons inside the sample the RFSE signal amplitude $A(T)$ is related to the SR $\nu = \nu_0 + \nu(T)$ (ν_0 from impurities and $\nu(T)$ from temperature dependent mechanisms) by the expression

$$A = A(0)\exp\{-\nu(T)t\} \tag{3}$$

(valid if $\nu_0 t > 1$), where ν_0 is included in the RFSE amplitude $A(0)$ at 0 K and t is the crossing time, that is, a fraction of the cyclotron period. (3) has two different regimes.

(i) At low temperature where $\nu(T)t \ll 1$, $A \approx A(0)\{1 - \nu(T)t\}$ a high-stability oscillator and high-resolution measurements are necessary to extract the correct $\nu(T)$. The extrapolation to $T = 0$ K to obtain $A(0)$ may be avoided by differentiating $A(T)$, which also requires a high precision.

(ii) At higher temperature (~5–10 K) when $\nu(T)t \gg 1$, the signal decreases rapidly and the temperature stability is a greater concern. Correlation with a reference signal taken at low temperature is the best way to extract the signal amplitude when the signal to noise ratio is small.

The sample is located in an RF coil, which is part of a tank circuit driven by a room temperature marginal oscillator (Probst *et al* 1977, Stubi *et al* 1988b). The oscillation amplitude and frequency are affected by any change in the complex surface impedance Z of the sample. A low-frequency modulation magnetic field B_m is added to the DC field B that selects the group of electrons to be studied, in order to use synchronous detection of $\partial Z/\partial B$. The modulation frequency is chosen low enough to ensure proper penetration of B_m in the sample (MacInnes *et al* 1977) and to avoid Joule heating. 3 Hz was found to be appropriate, without adding too much $1/f$ noise from the oscillator. To first order the detected amplitude is proportional to B_m, which needs to be stabilized at the 10^{-5} level. To do so, we had to develop a two-channel digital lock-in amplifier built as a Lab View† virtual instrument. One channel measures $\partial Z/\partial B$ and the other B_m, which is controlled within ± 20 ppm.

3.3. The digital lock-in amplifier

This instrument is described in detail in a separate publication (Probst and Jaquier 1994) and we shall only sketch here some basic points and characteristics. A sinewave signal of frequency f_{ref} is generated by scanning a sinetable at frequency f_{out} via direct memory access. Two or more input channels are sampled synchronously with the sinewave at a rate f_{in}, which depends on the analogue to digital board and the power of the computer behind.

† Lab View, NB-MIO-16X, NB-DMA 2800 by National Instrument Corporation.

With a Macintosh IIci, f_{out} up to 80 ks s^{-1} and f_{in} up to 10 ks s^{-1} allow extraction in real time of the amplitudes in phase and in quadrature with the f_{ref} signal for two channels. The stability of this instrument using MIO-16X and DMA2800 boards is within ±20 ppm for 24 h better than in any commercial lock-in amplifier.

The overall set-up and sample holder used in the present investigation have been described previously (Probst and Rittener 1989, Stubi *et al* 1988a, b). The temperature range of the measurements, 0.2–10 K, is obtained by means of a dilution refrigerator and the temperature is measured by Ge resistors; the magnetic field is small enough to limit to 1 mK the error due to the magnetoresistance in the sensors. The resistances are measured simultaneously and feedbacks are injected into heaters to stabilize the temperature at various points. A PID regulator cannot control a dilution refrigerator with the same parameters over the whole temperature range. We use the Ziegler–Nichols algorithm to optimize the parameters in each regime: gaseous flow above 4 K, normal liquid down to 2 K, superfluid down to 0.8 K and phase separation below. Above 2 K the temperature gradients in the system are minimized by controlling not only the mixing chamber temperature but also the still and the '1 K pot', the last two being 0.2 K colder than the mixing chamber, enough to have the required cooling power.

4. Experimental results

We have investigated the temperature dependence of the SRs on a few orbits of the second and third sheets of the FS with the best possible coupling between the electrons and the electric RF field, corresponding to the more favourable signal to noise ratio. The experimental conditions are such (see table 1) that the simple expression (3) can be used to determine the SR.

Before describing the results in relation to scattering, we shall first discuss the difficulties associated with some traces from charge carriers on the second zone, in order to be able to choose the correct orientations of $\boldsymbol{B}$, which make a proper determination of the SRs possible.

4.1. The anomalous T dependence of some RFSE amplitudes

Typical traces taken in sample Al 438 ($d = 438$ μm) for orbits on the second zone of the FS are shown in figure 2, with the magnetic field $\boldsymbol{B}$ tilted up to 6° away from the direction ⟨100⟩. The way the traces merge together when the field approaches this direction suggests that the signal for $\boldsymbol{B}$ exactly along ⟨100⟩ results from the superposition of signals from a few nearby orbits.

Possible orbits a_1, a_2 and a_3, whose resonance signals may overlap for this field direction, are drawn on the second band sheet of the FS in figure 3.

We have represented in figure 4 the temperature dependence of the amplitude of the RFSE resonances shown in figure 2, as ln $A(T)$ against T^3 in order to compare with the simple power law, together with data on two orbits on the third zone and a set of data by Parsons and Steele (1979). Such a representation obviously gives little weight to the measurements below 4 K, which tend to pile up near the T axis. One sees in this figure that the results for $\boldsymbol{B} \parallel \langle 100 \rangle$ exhibit a drop of the amplitude below 4.5 K. The same observation was made in In, which has a very similar FS (Hoff and de Groot 1978, Hoff 1977). As seen in figure 4 the decrease in the amplitude diminishes when the field is tilted until it disappears completely. ln A versus T^3 for a tilt angle of 6° can indeed be fitted by a straight line. For the two orbits on the third zone ln A is also linear in T^3, but with a much steeper slope, corresponding to a much larger temperature dependent SR.

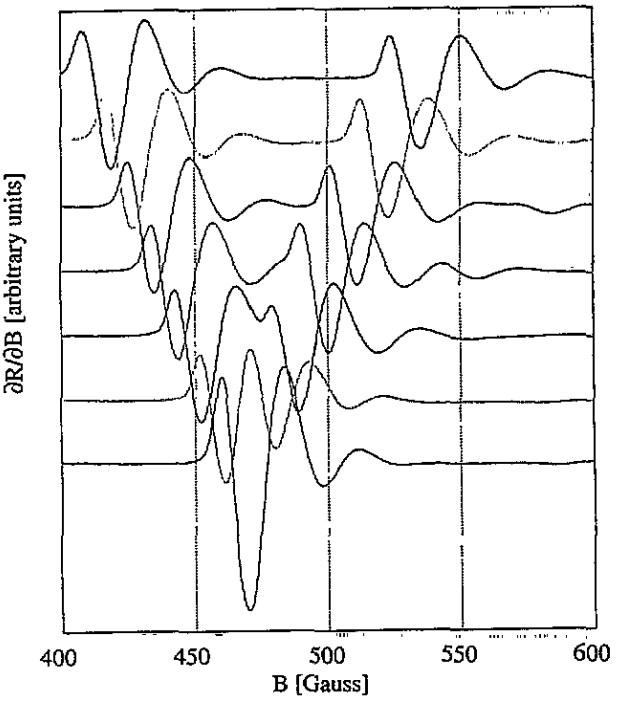

Figure 2. Traces from charge carriers on the second zone of Al taken at various angles θ (0, 1, 2, ..., 6°) of the magnetic field relative to the surface of the sample. The lowest curve is at $\theta = 0$ and corresponds to the ordinary RFSE parallel field geometry with $\boldsymbol{B} \parallel \langle 100 \rangle$; for this angle two or three orbits give overlapping resonance signals.

The topology of the FS of Al is such that the coupling between the RF field and the electrons is only favourable in a few orientations of the magnetic field $\boldsymbol{B}$. For these $\boldsymbol{B}$ directions, there may be many overlapping RFSE signals, due to central, non-central or partial orbits. Tilting the field away may destroy the overlap and new peaks will show up, as clearly demonstrated in figure 2. The model used to calculate the SR is of great help here. It allows one to find trajectories in $\boldsymbol{k}$ and $\boldsymbol{r}$ space and to calculate the resonance field B_c and its dependence upon the tilt angle, as well as crossing times and orbitally averaged SRs.

It is then quite easy to simulate the observed T dependence of a complex signal by summing the amplitudes of calculated SRs with slightly different temperature dependences, the only free parameter being the relative amplitude of the interfering signals. This has been done in figure 4, where the curve through Parsons and Steele's data for $\boldsymbol{B}$ exactly along $\langle 100 \rangle$ is calculated as the sum of overlapping signals from the orbits a_1 and a_2 of figure 3.

The good agreement between the calculated solid curve with the experimental data in figure 4, together with the merging out of the resonances in figure 2 when the magnetic field $\boldsymbol{B}$ is tilted away from the direction $\langle 100 \rangle$, demonstrate quite convincingly the origin of the decrease of $A(T)$ at low temperature when the temperature decreases. An alternative explanation has been proposed recently (Gasparov and Huguenin 1993), based on an apparent change in specularity of the sample due to an increasing electron mean free path when temperature decreases. While this explanation applies in the case of W, where electropolishing produces mirror-like sample surfaces, it has to be ruled out in our Al samples; the chemical etching used to remove the surface damage from mechanical polishing

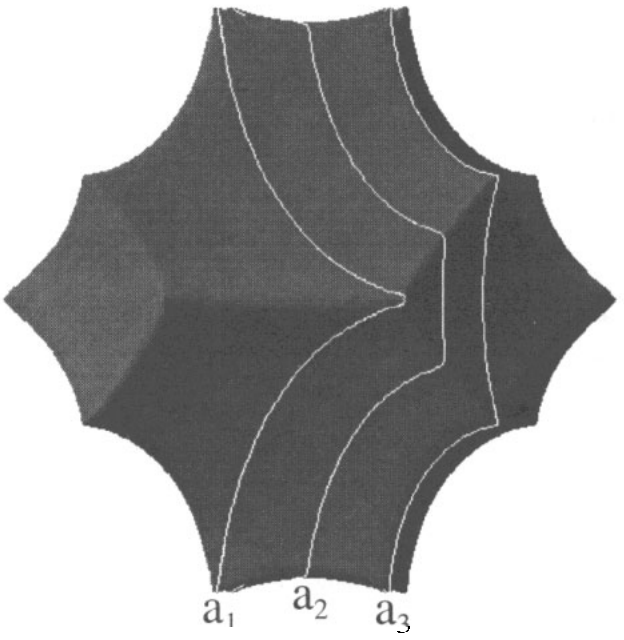

Figure 3. The second band sheet of the FS of Al with orbits a_1, a_2 and a_3, which may produce overlapping resonance signals.

probably produced rough surfaces, so that surface scattering was always diffuse. Which interpretation is correct in a particular metal and sample depends on the relative importance of the two effects, and this can only be tested by experiment.

4.2. Scattering rates

We have seen that the FS model allows the selection of RFSE signals due to one orbit only and from now on all the data we shall present are for such orbits. The temperature dependent SR is determined from (3) as

$$\nu(T) = (1/t)\ln[A(0)/A(T)]. \tag{4}$$

Let us assume that $\nu(T)$ results from the superposition of a T^2 term from e–e scattering (see section 2) and a term from e–p scattering $\nu_{ep}(T)$:

$$\nu(T) = \alpha T^2 + \nu_{ep}(T) \tag{5}$$

$\nu_{ep}(T)$ being in the simplest case proportional to T^3, as is realized in many experimental data. We shall choose to represent our data as $\nu(T)/T^2$ against T in order to give them equal weight at all temperatures, in contrast with the $\nu(T)$ versus T^3 representation of figure 4. This reduces to

$$\nu(T)/T^2 = \alpha + \beta T \tag{6}$$

when $\nu_{ep}(T) \propto T^3$.

In figure 5(*a*) we have represented the data for the simple orbit obtained with $\boldsymbol{B} \parallel \langle 100\rangle + 6°$ and measured in Al 610 ($d = 610$ μm) at the RF of 2.6 MHz and in Al 438 ($d = 438$ μm) at 0.8 MHz. It is seen that the latter data show a strong reduction of the e–p scattering compared to the former, which are aligned on a straight line over the

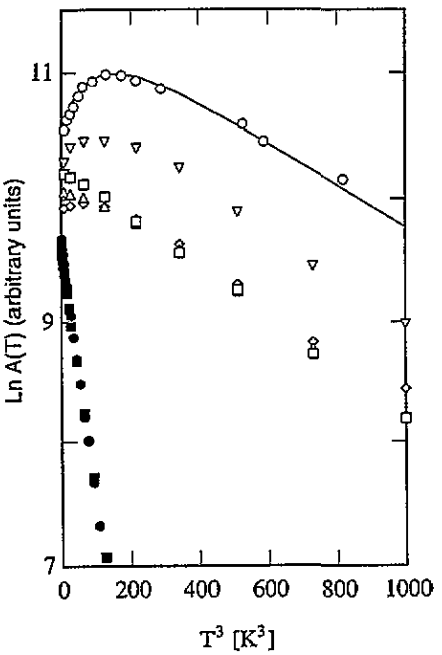

Figure 4. The logarithmic of the amplitude versus T^3 for different orbits; ○, Parsons and Steele (1979). The solid curve is the sum of two contributions with different T dependences. From the present work, sample Al 438 with $B \parallel \langle 100\rangle + \theta$: ▽, second zone, $\theta = 0$; ◇, second zone, $\theta = 2°$; △, second zone, $\theta = 4°$; □, second zone, $\theta = 6°$; ■, third zone, $B \parallel \langle 100\rangle$ and ●, third zone, $B \parallel \langle 110\rangle$.

whole temperature range of the measurements. Moreover $\nu(T)/T^2$ in the measurements at 0.8 MHz remains almost constant below about 2 K and the scatter of the low-temperature points is much small than in the 2.6 MHz data, because of a larger signal amplitude and a better signal to noise ratio. We recall that the RF was reduced intentionally to facilitate the observation of α in the right-hand side of (6) (see subsection 2.2). In figure 5(a) a straight line through the high-frequency data above 1 K has the same 0 K intercept with the vertical axis (see the arrow in figure 5(a)) as the low-frequency data taken on the thinner sample. We remark here that the plot $\nu(T)/T^2$ against T requires a very high precision on the measured amplitudes at low temperature, an error of 10^{-4} on the amplitude producing a 30% error on $\nu(T)/T^2$ at 0.2 K.

Figure 5(b) shows the same plot as figure 5(a) but for the SRs on the third zone of the FS. One should notice the large difference in the vertical scales between these two figures, the SRs on the third zone being a factor of five larger than on the free-electron-like second zone. The temperature range where amplitudes can be measured is limited here to 6 K. In figure 5(b) all the data are close together, irrespective of the thickness of the samples and of the RF used. Because of the smallness of the third-zone dimensions, electron scattering is always effective and is not sensitive to the ratio δ/d in the range of the thickness and frequency used in the present measurements (see subsection 2.2). Surprisingly the intercept with the vertical axis, i.e. the extrapolation of $\nu(T)/T^2$ to 0 K, measuring α in (6), is about an order of magnitude larger than for charge carriers on the second zone. We will see that this order of magnitude difference cannot be explained by ordinary Coulomb interaction between the electrons.

Although the representation of $\nu(T)/T^2$ against T in figures 5(a) and (b) is quite

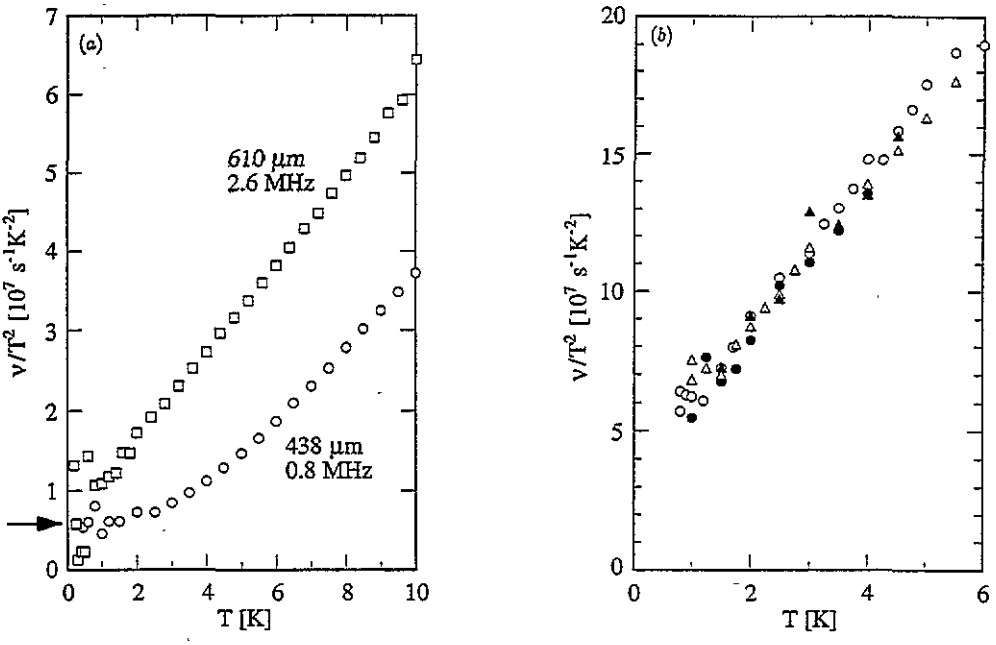

Figure 5. The SR divided by T^2 against T (a) for the orbit with $B \parallel \langle 100\rangle + 6^\circ$ on the second zone, □, Al 610, RF = 2.6 MHz and ○, Al 438, RF = 0.8 MHz; (b) the third-zone orbit, Al 438, $B \parallel \langle 100\rangle$, ●, RF = 2.6 MHz and ○, RF = 0.8 MHz; $B \parallel \langle 110\rangle$, ▲, 2.6 MHz and △, 0.8 MHz.

appropriate to show the existence of a T^2 term, it has the important drawback of requiring the extrapolation of the data to 0 K to obtain the amplitude $A(0)$ in (2) for determining the SR. This is not an extremely serious difficulty when the temperature range extends down to 0.2 K. However for the third-zone electrons, the RFSE resonance occurs at about 40 G and the superconducting transition temperature at this field is 0.8 K, preventing any observation below this temperature. In any case one can avoid the extrapolation by calculating the derivatives $\mathrm{d}(\ln A)/\mathrm{d}T$ of the raw data. From (3) and (4) it follows that

$$(1/2tT)\,\mathrm{d}(\ln A(T))/\mathrm{d}T = (1/2T)\,\mathrm{d}\nu/\mathrm{d}T = \alpha + (1/2T)\,\mathrm{d}\nu_{\mathrm{ep}}/\mathrm{d}T \qquad (7)$$

and in this representation the intercept with the vertical axis measures directly the first term α in the right-hand side of (7). The results are shown in figure 6(a) and (b) for the data plotted in figure 5(a) and (b). As expected for a derivative the points show more scatter but it is quite satisfactory that this representation reproduces very nearly the same values of the intercepts with the vertical axis, that is the same values of α as obtained from figure 5(a) and (b), completely supporting the previous analysis.

5. Discussion

In the measurements of Parsons and Steele in the tilted field geometry (Parsons and Steele 1979), where the SR was unambiguously related to the RFSE signal amplitude, the resolution was not sufficient to trace various contributions to the SRs, while the reported T^n law with $n \simeq 2.5$ suggests that a T^2 term was possibly present. To our knowledge the only other experimental data for Al are those of Wegehaupt and Doezema, who used SLL resonances in a large temperature interval, from 4 K to 20 K, and found that the SRs followed a T^3 law, irrespective of the position on the FS, with no sign of a T^2 component (Wegehaupt and

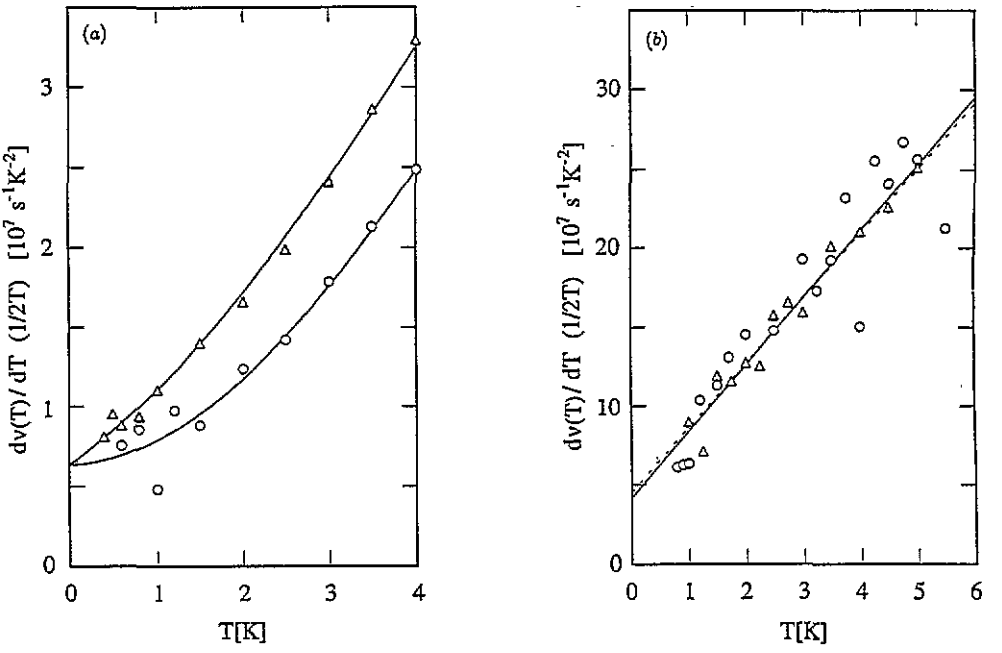

Figure 6. The derivative of $\nu(T)$ divided by $2T$ against T (equation (7)): (*a*) second-zone orbit, sample Al 438, $B \parallel \langle 100\rangle + 6°$, △, RF = 2.6 MHz, ○, RF = 0.8 MHz; (*b*) third-zone orbit, sample Al 438, RF 0.8 MHz, ○, $B \parallel \langle 100\rangle$, △, $B \parallel \langle 110\rangle$.

Doezema 1978). One must recall that theory predicts such a term—observed in electrical resistivity measurements—and a complicated temperature dependence of $\nu_{ep}(T)$. That no T^2 component was detected is not too surprising as it would only amount to 10% of the total SR at 10 K and 5% at 20 K if $\alpha \simeq \beta$. It is more difficult to explain why no point SR showed deviations from T^3. This may be connected with the somewhat indirect way the SR is determined through the width of the SLL resonance signals.

5.1. e–p scattering

As mentioned above the primary goal of the present work is e–e scattering. Before one can hope however to observe the e–e SR one needs to have a good understanding of e–p scattering in the particular metal investigated. One can then choose the necessary experimental conditions in order to facilitate the separation of the two scattering mechanisms. For these reasons we shall first discuss e–p scattering.

The simplest behaviour in our data is exhibited by the SR of the second-zone orbit with $B \parallel \langle 100\rangle + 6°$ at the highest RF used, i.e. 2.6 MHz. Nevertheless it is surprising that the data follow so well the T^3 law, as observed in many metals, while theory predicts a much more complicated behaviour in Al. We are now in a position to compare our experimental data with recent first-principles calculations (Jaquier 1994). For this comparison the theoretical point SRs $\nu(k)$ have of course to be averaged over the orbit considered according to

$$\bar{\nu} = \left(\int \frac{\mathrm{d}k}{v_\perp} \nu(k) \right) \Big/ \int \frac{\mathrm{d}k}{v_\perp} \tag{8}$$

and in addition one has to account for the energy dependence of the SR (see subsection 2.2).

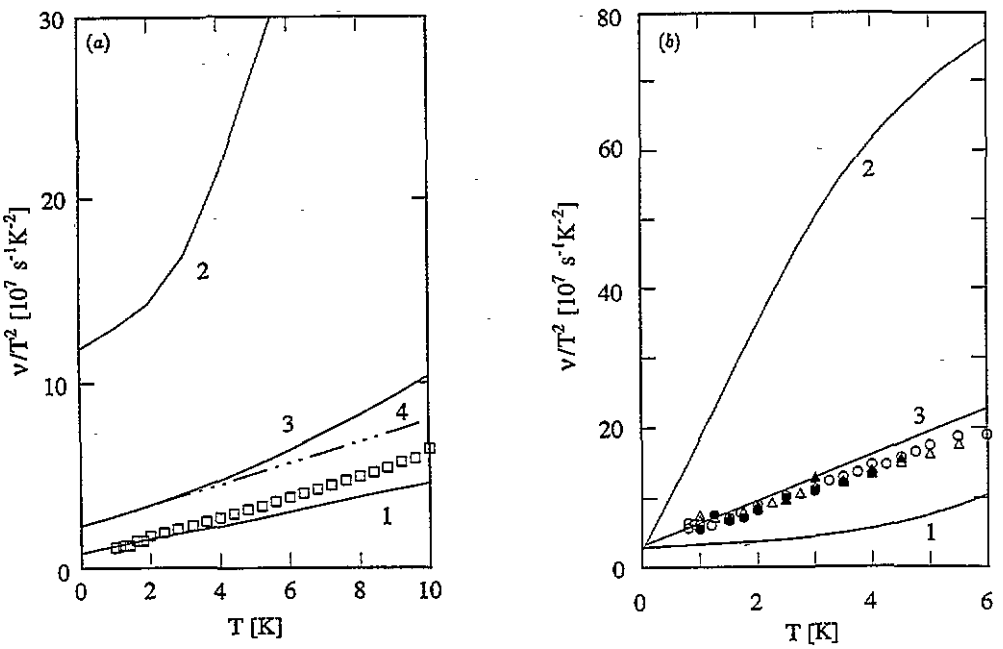

Figure 7. A comparison of $\nu(T)/T^2$ from experiment (symbols) and theory (curves) (see the text): *(a) second-zone orbit; (b) third-zone orbit (the calculated e–p SRs are unrenormalized).*

Figure 7 shows that the e–p scattering is indeed well understood in Al. The measured $\nu(T)/T^2$ is plotted against T in figure 7(a) for the above-mentioned orbit and in figure 7(b) for orbits on the third zone, together with theoretical results.

The theoretical curves 1 and 2 in figure 7(a) are for point SRs at the Fermi level, respectively for k near ⟨111⟩ and k on the ridge between the hexagonal and square faces of the FS (see figure 2). They exhibit extreme behaviours, that is near ⟨111⟩ the electrons are essentially free and this is reflected in the lowest SR and in the simplest T dependence, while on the ridge the SR is an order of magnitude larger and the T dependence strongly deviates from the T^3 law. Curve 3 is obtained when one averages the calculated point SRs over the orbit corresponding to the experimental data and multiplies the result by $\frac{12}{7}$ to account roughly for energy dependence. In doing so we assume that electrons of all energies participate in the formation of the RFSE resonance. The completed curve 3 is however curved upwards while the experimental data are linear in T. This straight line behaviour can be understood by a more correct theoretical treatment of the energy averaging. According to (2) the energy averaging depends upon the time the charge carriers spend on the various parts of the orbit. At the lowest temperatures of the measurements all the electrons within $\pm k_B T$ of ε_F will participate in the formation of the resonance signal (leading to the factor $\frac{12}{7}$) whereas eventually only electrons at the Fermi level will be able to do so at the highest temperatures. To account for the slow changing over from one situation to the other one has to use the more realistic procedure included in (1). We then obtain curve 4, which is nicely parallel to the experimental data. The offset on the vertical axis will be discussed in the next section below.

So it appears that energy averaging changes the temperature dependence of the average SR: as seen in figure 7(a) it may produce a T^3 law from complicated T dependences, curve 3 being changed to curve 4. One should therefore not be too surprised if cubic

temperature dependences have been observed in most previous works, while theory almost invariably predicts other powers of T. This point has also been discussed by Wegehaupt and Doezema, whole SLL experimental results were incapable of confirming predicted T^3 departures (Wegehaupt and Doezema 1978).

The same comparison is carried out in figure 7(*b*) for the electrons on the third zone. Here too the calculated local SRs exhibit a variety of behaviours, as seen in curves 1 and 2. Averaging over the measured orbits reproduces again very well the experimental data, the calculated T^3 coefficient (curve 3) being only about 20% larger than the measured one, that is 3.2×10^7 (renormalized 2.2×10^7) instead of 2.6×10^7. On this orbit scattering is much stronger than on the second zone and the experiment only measures the SR of electrons at the Fermi level, so no effect from energy averaging is detected, even in the lower part of the temperature range of the measurements.

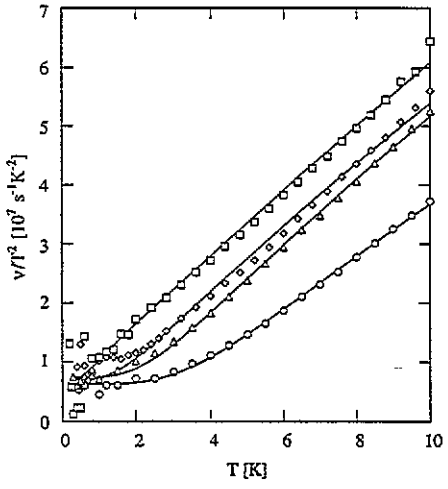

Figure 8. $\nu(T)/T^2$ against T for the second-zone orbits, $B \parallel \langle 100 \rangle + 6°$: Al 610, □, RF = 2.6 MHz, ◇, RF = 0.8 MHz; Al 438, △, RF = 2.6 MHz, ○, RF = 0.8 MHz. The curves through the experimental data are calculated with expression (9).

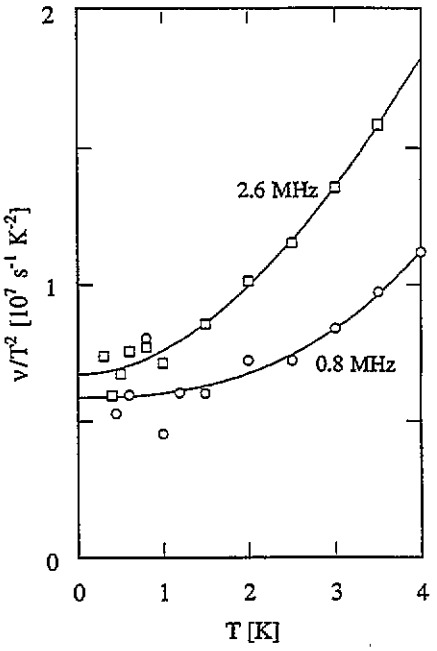

Figure 9. ν/T^2 against T in sample Al 438 below 4 K.

While there is no sign of ineffective e–p scattering for the electrons of the third zone we have seen in figure 5 that this is not the case for the second-zone holes. We have replotted in figure 8 $\nu(T)/T^2$ against T for second-zone holes, measured under various conditions, for comparison with theoretical calculations. Ineffectiveness is accounted for by means of the simplest expression used by Stubi *et al* to interpret their data in the noble metals (Stubi *et al* 1988b). In this model the e–p SR at the Fermi level reads

$$\nu(T) = \beta T^3 \int_{T_\Sigma/T}^{\infty} \mathrm{d}x \frac{x^2 e^x}{e^{2x} - 1} \frac{4}{7\zeta(3)} \tag{9}$$

where $x = \hbar qs/k_B T$ (s is the sound velocity). T_Σ is the temperature where the RMS amplitude of the phonon wave vector $q_{RMS} = (k_B/4.15\hbar s)T$ is equal to the dimension of the region of the FS perturbed by the RF electric field. The inverse of numerical factor $4/7\zeta(3)$ is the value of the integral from 0 to ∞. In this model scattering is totally ineffective when $T \to 0$ K while at higher temperature $\nu_{ep}(T)$ is again proportional to T^3. The crossover temperature T_Σ depends upon the ratio δ/d (skin depth/sample thickness), which is proportional to $1/\omega^{1/3}$ in the anomalous regime.

Table 2. Parameters of e–p scattering in (9).

	β (10^6 s^{-1}K^{-3}) experiment: fits to (9)	β (10^6 s^{-1}K^{-3}) theory	T_Σ (K)	δ/d (10^{-3})
Al 438 0.8 MHz	3.8	4.2	14.2	9.5
Al 438 2.6 MHz	4.9	4.2	9.3	6.3
Al 610 0.8 MHz	4.9	4.2	6.2	5.6
Al 610 2.6 MHz	5.4	4.2	2.1	3.6

The solid curves in figure 8 are calculated from the ineffectiveness model (equation (9)) with β and T_Σ as adjustable parameters (table 2). These reproduce very well the experimental data. As expected, in the 610 μm thick sample and at the highest RF used, 2.6 MHz, almost all the collisions are effective and there is very little difference between the curves computed with $T_\Sigma = 2.1$ and $T_\Sigma = 0$ (all scatters effective). Reducing the RF to 0.8 MHz decreases systematically the SRs. In the thinner sample, $d = 438$ μm, ineffectiveness is already present at 2.6 MHz and the effect increases when the RF is diminished to 0.8 MHz. In the present work we were particularly interested in using a reduced frequency in order to reduce the effectiveness of e–p scattering, this making the determination of e–e scattering easier.

Although the curves calculated with (9) reproduce the experimental data extremely well over the whole temperature range of the measurements, the physical parameters β and T_Σ listed in table 2 have to be considered cautiously, as they are obtained under quite simple assumptions. T_Σ correctly increases with the ratio δ/d, but β from the fits (the second column in table 2) should of course be a constant. It is worth mentioning that in Al a factor of three increase in δ/d changes totally effective scattering into almost totally ineffective scattering below about 2 K, while this ratio had to be changed by more than 10 to produce the same effect in the noble metals. This is probably due to the shape of the FS of Al.

5.2. e–e scattering

We have seen that figures 5, 6 and 8 clearly demonstrate the existence of a T^2 term, which adds to the e–p SR discussed above. The determination of α is made easier by the reduction of e–p scattering when the RF is made smaller, as $\nu(T)/T^2$ then tends at low temperature to a plateau, resulting in a clear intercept, which measures α. This is clearly seen in figure 9, where the data below 4 K for sample Al 438 at 2.6 and 0.8 MHz are represented. The two methods used to determine α, either from $\nu(T)/T^2$ at different RFs or from the derivatives of $\nu(T)$ divided by T, give very nearly the same values; these are listed in table 3 together with theoretical estimates from various sources and from resistivity measurements.

Our measurements are the first to show the presence in Al of a T^2 contribution in $\nu(T)$ as directly measured by means of a probe looking at selected groups of charge carriers, SLL or RFSE. However we mentioned above that resistivity data (Ribot *et al* 1981) can be analysed as

$$\rho(T) = AT^2 + BT^5 \tag{10}$$

Table 3. A comparison of measured and calculated T^2 coefficients in Al in $\nu_{ee} = \alpha T^2$.

	α (10^7 s^{-1} K^{-2}) *experiment*	α (10^7 s^{-1} K^{-2}) *theory*
Orbits		
second zone $B \parallel \langle 100 \rangle + 6°$	0.68 ± 0.05	2.2[a]
third zone $B \parallel \langle 100 \rangle$	1.9 ± 0.5	3.8[a]
third zone $B \parallel \langle 110 \rangle$	2.6 ± 0.5	3.9[a]
local orbits near point L		0.9[a]
FS averages		
electrical resistivity		
T range 1.2–2.8 K	3.6[b]	
T range 2.8–4 K	5.3[c]	
theory		
Lawrence and Wilkins		0.15[d]
MacDonald and Geldart		5.3[e]
Schwartzman and Lawrence		1.6[f]
Jaquier *et al*		2.8[a]

[a] Jaquier *et al* (1994), Jaquier (1994).
[b] Measured e–e resistivity and formula (10) (Ribot *et al* 1981).
[c] Measured e–e resistivity and formula (10) (Hou and Kos 1993).
[d] Coulomb e–e resistivity and formula (10) (Lawrence and Wilkins 1973).
[e] Phonon mediated e–e resistivity and formula (10) (MacDonald and Geldart 1980).
[f] Phonon mediated e–e SR (Schwartzman and Lawrence 1993).

between 1.2 and 2.8 K, the AT^2 being attributed to e–e scattering. The value of A obtained by Ribot *et al* amounts to 2.8×10^{-15} Ω m K^{-2}, which corresponds to an e–e SR

$$\nu_{ee} = \left[(ne^2/m)\Delta\right]AT^2 = \alpha T^2 \tag{11}$$

where n is the electron concentration, m and e the electron mass and charge, and Δ the fraction of umklapp to total scattering. In the free electron model, with the electron concentration of Al, $n = 18.1 \times 10^{28}$ m^{-3}, and with $\Delta = \frac{2}{5}$ as estimated for this metal by Lawrence (1976) one obtains

$$\alpha = \left[(ne^2/m)\Delta\right]A = 3.6 \times 10^7 \ \Omega \text{ m } K^{-2}.$$

One can see in table 3 that the values of α measured on the three orbits investigated here are smaller than the values calculated by Jaquier *et al* (1994) and Jaquier (1994) for the same orbits, namely a factor of three on the second zone, a factor of two on the third zone with $B \parallel \langle 100 \rangle$ and 50% on the third zone with $B \parallel \langle 110 \rangle$.

The orbit with $B \parallel \langle 100 \rangle + 6°$ runs over large free-electron-like parts of the FS (see figure 3) where the local α is 0.9×10^7 s^{-1} K^{-2}, that is, 30% larger than measured for the whole orbit, and it is somewhat surprising that the theoretical orbital averaged α is so large (the first row in table 3). There are indeed no obvious reasons why the regions between the hexagonal and the square faces of the FS—where the calculated α is very high—should not contribute to the orbital average. Unfortunately these regions are not experimentally accessible, because of the shape of the FS and the finite region of the FS perturbed by the RF field, either in SLL experiments or RFSE experiments in a tilted magnetic field. Notwithstanding, in view of the difficulties associated with the calculation of the phonon mediated e–e SR, made without any free parameters, the overall agreement can be considered as quite fair. The values of α compare also well with previous theoretical results (MacDonald and Geldart 1980, Schwartzman and Lawrence 1993), as well as with the electrical resistivity results (Ribot *et al* 1981, Hou and Kos 1993).

One should also notice that the direct e–e Coulomb interaction produces values of α a factor of 10 smaller (MacDonald 1980), so there is little doubt that the large contribution

from e–e scattering in Al, either in the bare SR or in the electrical resistivity, is due to phonon mediation as first suggested by MacDonald. This is also supported by the anisotropy of α, both from experiment and theory.

Table 4. A comparison of values of α from experiment and theory in various metals (in 10^7 s^{-1} K^{-2}).

	Experiment	Theory
Al RFSE orbital averages	0.68–2.6[a]	2.2–3.9[b]
Al RFSE point SRS		1–22[b]
Mo	1.3–2.9[c]	2.3[d]
W	0.54–1.1[e]	0.9–1.3[f]
Cd	0.8[g]	0.8[d]
Cu	0.20–0.25[h]	0.24[d]
Ag	0.1–0.17[h]	0.07[d]

[a] This work.
[b] Jaquier *et al* (1994), Jaquier (1994).
[c] Gasparov *et al* (1979).
[d] Schwartzman and Lawrence (1993).
[e] Van der Maas *et al* (1985).
[f] Potter and Morgan (1979).
[g] Jaquier *et al* (1991).
[h] Stubi *et al* (1988a).

It is interesting to note that the value of α measured on the second-zone orbit of Al, close to the theoretical value predicted on the free-electron-like parts of the FS near point L, is also quite close to what has been measured in the superconducting Cd or in the transition metals Mo and W. It is a factor of five larger than in the non-superconducting noble metals Cu and Ag, where the e–e phonon mediation plays a negligible role. The values obtained to date in various metals are listed for comparison in table 4.

6. Conclusion

For the first time we have been able to observe T^2 terms in the temperature dependent scattering rate of Al, which may be interpreted as a result of the e–e interaction and which reconciles the RFSE data with previous electrical resistivity results. The coefficient α of the T^2 term is anisotropic, and quite large even for electrons on the second zone of the FS. Both the order of magnitude of α and its anisotropy give strong support for the argument that this term originates essentially from phonon mediated e–e interaction. The Coulomb interaction between the electrons would be expected to produce a smaller value of α and much less anisotropy. The observed values are found to be in reasonable agreement with the results of a recent first-principles calculation (Jaquier *et al* (1994), Jaquier 1994).

The experimental data also agree very closely with the first-principles calculation of the e–p contribution to the scattering rate at the Fermi level, provided that account is taken of critical factors linked to the experimental conditions. These factors are the energy dependence of the scattering rate and the scattering ineffectiveness. Both of these can alter the temperature dependence of the e–p scattering rate in a manner that depends upon the sample thickness and the RF used. Fortunately these effects can be accounted for by simple models. In particular, scattering ineffectiveness has been exploited as a tool to clearly separate the e–e from the e–p contribution to the scattering rate. We also explain the anomalous temperature dependence previously observed, in Al and In, by the overlap of signals from two or three nearby orbits.

Acknowledgments

We are grateful to W E Lawrence for a critical reading of the manuscript and for many valuable suggestions and to the Swiss National Foundation for Scientific Research for financial support.

References

Ashcroft N W 1963 *Phil. Mag.* **8** 2055
Baber W G 1937 *Proc. R. Soc.* A **158** 383
Boiko V V, Gantmakher V F and Gasparov V A 1974 *Sov. Phys.–JETP* **38** 604
Gantmakher V F 1974 *Rep. Prog. Phys.* **37** 317
Gasparov V A and Harutunian M M 1976 *Solid State Commun.* **19** 189
Gasparov V A and Huguenin R 1993 *Adv. Phys.* 4 393
Gasparov V A, Voloshin I F and Fisher L M 1979 *Solid State Commun.* **29** 43
Hartmann W M and Milbrodt T O 1971 *Phys. Rev.* B **3** 4133
Hoff A B M and de Groot D 1978 *J. Low Temp. Phys.* **33** 1
Hoff A B M 1977 *Thesis* Amsterdam University
Hou Y Z and Kos J F 1993 *J. Phys.: Condens. Matter* **5** 7797
Jaquier A 1994 *Thesis* Lausanne University
Jaquier A, Probst P A, Huguenin R, Stubi R and Lawrence W E 1994 *Physica* B **194–196** 1319
Jaquier A, Probst P A, Stubi R, Huguenin R and Lawrence W E 1991 *J. Phys.: Condens. Matter* **3** 10065
Kaveh M and Wiser N 1984 *Adv. Phys.* **33** 257
Landau L D and Pomeranchuk I Y 1936 *Phys. Z. Sowjetunion* **10** 649
Lawrence W E 1976 *Phys. Rev.* B **13** 5316
Lawrence W E and Wilkins J W 1972 *Phys. Rev.* B **6** 4466
—— 1973 *Phys. Rev.* B **7** 2317
MacDonald A H 1980 *Phys. Rev. Lett.* **44** 489
MacDonald A H and Geldart D J W 1980 *J. Phys. F: Met. Phys.* **10** 677
MacInnes W M, Collet B, Probst P A and Huguenin R 1977 *J. Phys. F: Met. Phys.* **7** 655
Meador A B and Lawrence W E 1977 *Phys. Rev.* B **15** 1850
Monnier R and Joss W 1980 *J. Phys. F: Met. Phys.* **10** 30
Parsons D and Steele C A 1979 *J. Phys. F: Met. Phys.* **9** 1783
Peercy P S, Walsh W M, Rupp L W and Schmidt P H 1968 *Phys. Rev.* **171** 713
Potter C and Morgan G J 1979 *J. Phys. F: Met. Phys.* **9** 493
Probst P A, Collet B and MacInnes W M 1977 *Rev. Sci. Instrum.* **47** 1522
Probst P A and Jaquier A 1994 *Rev. Sci. Instrum.* **65** 747
Probst P A and Rittener J 1989 *Helv. Phys. Acta* **62** 298
Ribot J H, Bass J, Van Kempen H, Van Vucht R J M and Wyder P 1981 *Phys. Rev.* B **23** 532
Schwartzman K and Lawrence W E 1993 *Phys. Rev.* B **48** 14089
Stubi R, Probst P A, Huguenin R and Gasparov V A 1988a *J. Phys. F: Met. Phys.* **18** 1211
—— 1988b *J. Phys. F: Met. Phys.* **18** 2429
Van der Maas J, Huguenin R and Gasparov V A 1985 *J. Phys. F: Met. Phys.* **15** L271
Wagner D K and Bowers R 1978 *Adv. Phys.* **27** 651
Wegehaupt T and Doezema R E 1978 *Phys. Rev.* B **18** 742